

This article was downloaded by:

On: 25 January 2011

Access details: *Access Details: Free Access*

Publisher *Taylor & Francis*

Informa Ltd Registered in England and Wales Registered Number: 1072954 Registered office: Mortimer House, 37-41 Mortimer Street, London W1T 3JH, UK



Liquid Crystals

Publication details, including instructions for authors and subscription information:

<http://www.informaworld.com/smpp/title~content=t713926090>

Synthesis and evaluation of some novel chiral heterocyclic liquid crystalline materials exhibiting ferro- and antiferro-electric phases

Robert McDonald^a; David Lacey^a; Paul Watson^a; Stephen Cowling^a; Paul Wilson^a

^a Department of Chemistry, University of Hull, East Yorkshire, HU6 7RX, UK

To cite this Article McDonald, Robert , Lacey, David , Watson, Paul , Cowling, Stephen and Wilson, Paul(2005) 'Synthesis and evaluation of some novel chiral heterocyclic liquid crystalline materials exhibiting ferro- and antiferro-electric phases', *Liquid Crystals*, 32: 3, 319 – 330

To link to this Article: DOI: 10.1080/02678290500033711

URL: <http://dx.doi.org/10.1080/02678290500033711>

PLEASE SCROLL DOWN FOR ARTICLE

Full terms and conditions of use: <http://www.informaworld.com/terms-and-conditions-of-access.pdf>

This article may be used for research, teaching and private study purposes. Any substantial or systematic reproduction, re-distribution, re-selling, loan or sub-licensing, systematic supply or distribution in any form to anyone is expressly forbidden.

The publisher does not give any warranty express or implied or make any representation that the contents will be complete or accurate or up to date. The accuracy of any instructions, formulae and drug doses should be independently verified with primary sources. The publisher shall not be liable for any loss, actions, claims, proceedings, demand or costs or damages whatsoever or howsoever caused arising directly or indirectly in connection with or arising out of the use of this material.

Synthesis and evaluation of some novel chiral heterocyclic liquid crystalline materials exhibiting ferro- and antiferro-electric phases

ROBERT MCDONALD, DAVID LACEY*, PAUL WATSON, STEPHEN COWLING and PAUL WILSON

Department of Chemistry, University of Hull, Hull, East Yorkshire, HU6 7RX, UK

(Received 30 April 2004; in final form 24 August 2004; accepted 26 September 2004)

Two series of three-ring heterocyclic liquid crystalline (LC) materials have been synthesized and characterized, one incorporating a thiophene ring and the other containing a thiophene-pyrimidine moiety. This is the first study to show the effect of a thiophene-pyrimidine moiety on the thermal and physical properties of a mesogen. The effect on the thermal stability of the mesogen by the introduction of the pyrimidine ring has been dramatic, with the thiophene-pyrimidine-containing mesogens exhibiting ferro- and antiferro-electric phases only. The introduction of the pyrimidine ring can be compared to the effect observed by lateral fluorination; a reduction in the melting point and smectic phase thermal stability of mesogens. However, its introduction is also conducive to the formation of the SmC* (ferro- and antiferro-electric) phase. Like the fluoro substituent, the pyrimidine ring could play a key role in tailoring important thermal and physical properties of LC materials. An electro-optical study not only showed that the incorporation of a pyrimidine ring into the structure of a mesogen can produce mesogens with high P_s values (200–230 nC cm⁻²) and tilt angles (41°–41.5°), but also helped to identify the SmC_x* phase exhibited by members of one of the series of compounds.

1. Introduction

We recently reported the synthesis and characterization of a large number of three-ring achiral heterocyclic LC materials that exhibited, amongst other phases, the SmC phase [1]. Before this work a great deal of research had been carried out on mesogens incorporating a pyrimidine ring [2–6], because it produces low viscosity mesogens exhibiting wide SmC ranges. Mesogens incorporating the thiophene ring have also been investigated, the ‘bent’ nature of the molecule (due to the presence of the thiophene ring) leading to mesogens with fairly low melting points and extensive SmC ranges [7–10]. However, the work reported in [1] was the first to incorporate the thiophene-pyrimidine moiety in a mesogen structure and clearly showed that this moiety is conducive to the formation of tilted smectic phases, in particular the SmC phase. Due to the low melting points of these materials, many showed extensive SmC ranges.

In a continuation of our work on heterocyclic mesogens, we now describe the thermal and electro-optic results obtained for two series of optically active mesogens incorporating thiophene and the thiophene-pyrimidine moiety. The structures of these series 1 and 2 compounds are shown in figure 1. The main aim of this

work was to establish the effect on thermal and physical properties of a ferroelectric thiophene-containing chiral mesogen of replacing one of the benzene rings by a pyrimidine ring.

2. Results and discussion

The work involved the synthesis and evaluation of the thermal and physical properties of two series of three-ring, heterocyclic LC materials (see figure 1). Full experimental details are given in §4.

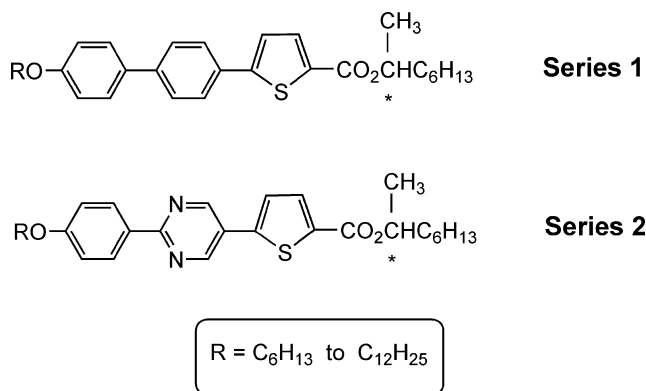
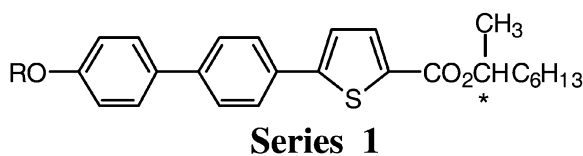


Figure 1. Structures of series 1 and 2 compounds.

*Corresponding author. Email: d.lacey@hull.ac.uk

Table 1. Transition temperatures ($^{\circ}\text{C}$) and enthalpies (in brackets, J g^{-1}) for series 1 compounds.

Compound <i>R</i>	Cr–SmC*, SmA*	SmI*–SmC*	SmC*–SmA*	SmA–I
7a C ₆ H ₁₃	118.0 (31.68)	[117.4] ^a (3.42)	123.0 (0.77)	147.1 (14.85)
7b C ₇ H ₁₅	123.9 (37.60)		126.2 (0.82)	138.4 (12.34)
7c C ₈ H ₁₇	125.4 (37.92)		127.0 (1.50)	135.2 (11.52)
7d C ₉ H ₁₉	127.9 (42.43)		[126.7] (2.26)	130.6 (10.52)
7e C ₁₀ H ₂₁	125.5 (40.02)		[125.1] (2.40)	127.9 (10.26)
7f C ₁₁ H ₂₃	123.1 (40.11)		[123.0] (2.91)	125.1 (9.35)
7g C ₁₂ H ₂₅	118.2 (32.52)		121.5 (2.40)	123.1 (8.70)

^a[] Denotes a monotropic transition.

2.1. Thermal properties of series 1 and 2 compounds

2.1.1. Series 1 compounds. The structure and thermal properties of series 1 compounds (**7a–g**) are given in table 1. A plot of transition temperature against the number of carbon atoms in the alkoxy chain *RO* is given in figure 2.

All the compounds in series 1 exhibit the SmA* and ferroelectric SmC* phase, with the hexyloxy homologue **7a** also exhibiting the SmI* phase. It can be seen from figure 2 that the SmA*–I transition temperatures lie on two sharply descending, converging curves; the upper curve representing the even members of the homologous series and the lower curve the odd members. At around the decyloxy homologue **7e**, the curves finally meet. The

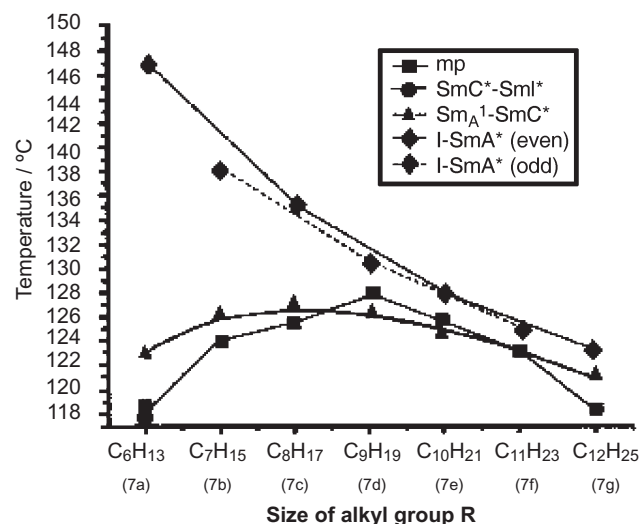


Figure 2. Plot of transition temperature against the size of the alkyl group *R* for series 1 compounds.

SmC*–SmA* transition temperatures all lie on a single smooth curve which rises as the length of the alkyl group *R* increases. At the octyloxy homologue **7c**, the curve levels out and then begins to fall gradually with increasing size of the *R* group. The SmC*–SmA* transition temperatures for compounds **7d–f** are all monotropic. The melting points for series 1 compounds are a little unusual in that those for the hexyloxy **7a** and dodecyloxy **7g** homologues are very similar but some 5–7 $^{\circ}\text{C}$ lower than the other homologues in the series, whose melting points differ only by 1–2 $^{\circ}\text{C}$.

The hexyloxy homologue **7a** is the only compound in this series to exhibit the SmI* phase, which is monotropic. Confirmation of this phase was achieved by optical microscopy on a free-standing film. Even using a free-standing film the SmI* phase was difficult to detect, as shown in figures 3(a, b). Figure 3(a) illustrates a free-standing film of the ferroelectric SmC* phase exhibited by compound **7a**, and is typical of that phase. In figure 3(b) we see the free-standing film of the SmC* for compound **7a** which shows in the lower half, centre, the transition bars for the SmC*–SmI* transition.

The phases exhibited by series 1 compounds were identified by optical microscopy but only the electro-optical study showed that members of the series, especially compounds **7d–g**, also exhibited the SmC_z* phase. This recently identified phase is extremely difficult to observe by optical microscopy; it is now believed to be present in many optically active LC materials. The structure of the phase is still uncertain but it is believed to be made up of both the ferroelectric 1 and ferroelectric 2 phases [11]. In the electro-optical study of such compounds, the SmC_z* phase appears as two small, progressively converging peaks on cooling.

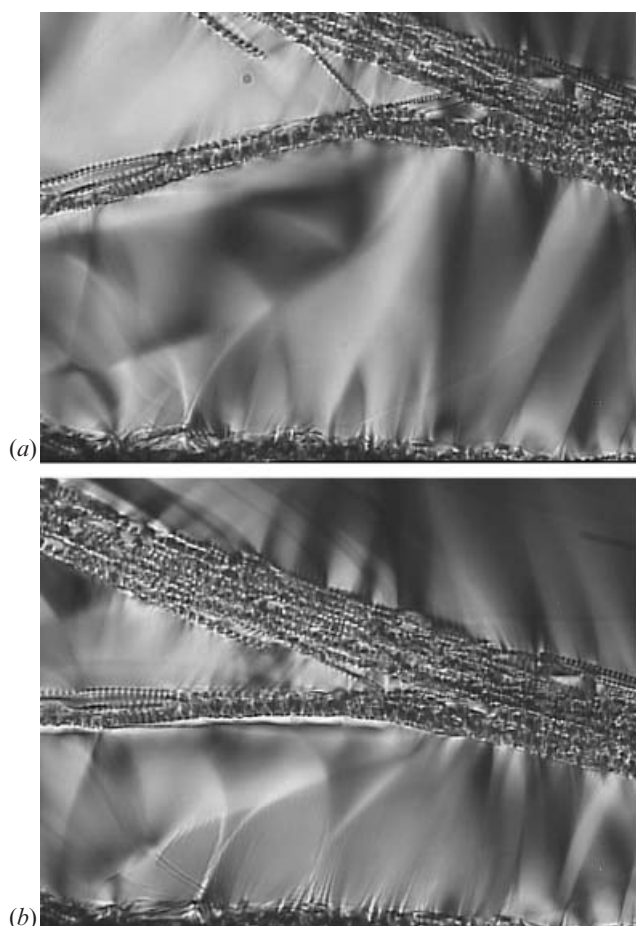


Figure 3. (a) Photomicrograph of free-standing film of the ferroelectric SmC^* phase exhibited by compound **7a**. (b) Photomicrograph of free-standing film of the SmC^* phase for compound **7a**; in the bottom half, near the centre, the SmC^* – SmI^* transition bars can just be seen.

This is shown in figure 4 for compound **7d**. The two peaks of the SmC_α^* phase converge on approaching the ferroelectric phase. At the transition from the SmC_α^* phase to the ferroelectric phase, a single peak is observed which is reminiscent of the ferroelectric phase. The phase range is very short, less than one degree, and appears just before the onset of the SmA^* phase.

Compounds **7a–c** also exhibit the SmC_α^* phase, but its existence is less clear than in the case for compounds **7d–g**. The peak observed for the ferroelectric phase for compound **7d** has two side bands which could indicate the presence of the SmC_α^* phase. If compounds **7a–c** do exhibit the SmC_α^* phase, it is very short ranged, less than 0.1°C .

2.1.2. Series 2 compounds. The structure and thermal properties for series 2 compounds (**8a–g**) are given in table 2. A plot of transition temperature against the

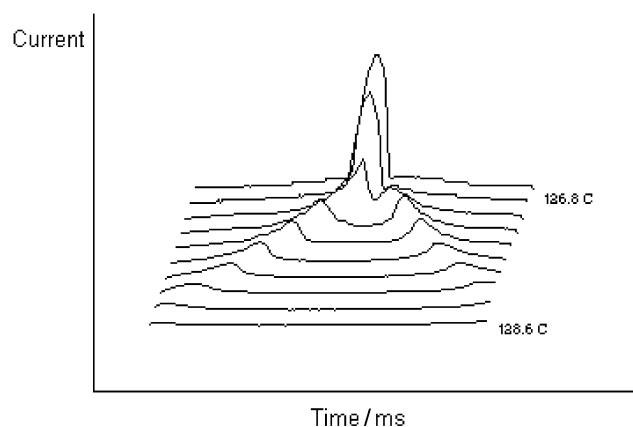


Figure 4. The electro-optical response of the SmC_α^* phase for compound **7d**.

number of carbon atoms in the alkoxy chain RO is given in figure 5.

In series 2 all the compounds exhibit either ferro- and/ or antiferro-electric SmC^* phases only. The hexyloxy to decyloxy compounds (**8a–e**) exhibit both ferro- and antiferro-electric phases, while the undecyloxy and the dodecyloxy homologues (**8f** and **8g**) exhibit the ferroelectric phase only. The ferroelectric SmC^* – I transition temperatures lie on two slightly descending, converging curves, which converge around the decyloxy homologue **8e**. However, the ferro- to antiferro-electric transition temperatures lie on two steeply descending curves as the length of the alkoxy group RO increases. This fall is so dramatic that beyond the decyloxy homologue only the ferroelectric SmC^* phase is observed. The melting points initially fall with increase in the length of RO , with the octyloxy **8c** homologue having a melting point below 70°C . This gives rise to

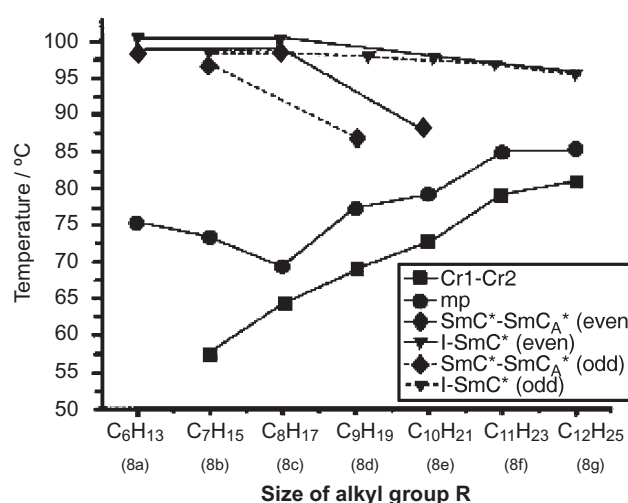
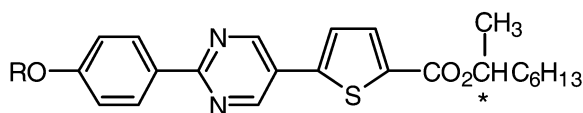


Figure 5. Plot of transition temperature against size of the alkyl group R for series 2 compounds.

Table 2. Transition temperatures ($^{\circ}\text{C}$) and enthalpies (in brackets, J g^{-1}) for series 2 compounds.

Series 2

Compound <i>R</i>	$\text{Cr}_1\text{-Cr}_2^{\text{a}}$	$\text{Cr}_2\text{-SmC}_A^*$, SmC^*	$\text{SmC}_A^*\text{-SmC}^*$	$\text{SmC}^*\text{-I}$
8a C_6H_{13}		75.2 (30.12)	98.9 ^b	99.8 (12.49)
8b C_7H_{15}	57.3 (2.91)	73.4 (27.74)	97.2 ^b	98.2 (12.21)
8c C_8H_{17}	64.1 (18.46)	69.3 (19.64)	98.8 ^b	99.8 (12.36)
8d C_9H_{19}	68.8 (3.21)	77.2 (25.90)	86.5 (0.014)	97.8 (11.71)
8e $\text{C}_{10}\text{H}_{21}$	72.4 (15.98)	79.0 (28.81)	87.1 (0.025)	97.6 (11.24)
8f $\text{C}_{11}\text{H}_{23}$	78.9 (7.41)	84.7 (34.87)		96.7 (11.81)
8g $\text{C}_{12}\text{H}_{25}$	80.7 (20.29)	85.6 (34.98)		95.3 (10.83)

^a $\text{Cr}_1\text{-Cr}_2$ is a crystal-crystal transition. ^bTransition could not be observed by DSC, only by optical microscopy.

large antiferroelectric SmC^* ranges for these three homologues; around 24°C for compounds **8a** and **8b**, but 29.6°C for compound **8c**. Beyond compound **8c**, the melting points steadily increase with increasing length of *RO*.

2.1.3. Comparisons between series 1 and series 2 compounds. From the data given in tables 1 and 2 it can be clearly seen that the introduction of a pyrimidine ring has had a dramatic effect on the thermal properties of series 2 compounds. The most obvious effect has been on the thermal stabilities of the smectic phases. Even in series 1 compounds the thermal stability of the SmA^* phase decreases sharply as the length of the alkoxy chain *RO* increases, probably due to the increasing effect of the 'bent' nature of the thiophene ring on the formation of the LC phases. However, the introduction of the pyrimidine ring has completely removed both the SmA^* and SmI^* (compound **7a**) phases.

One of the most significant differences between the two series of compounds is that those in series 1 exhibit the ferroelectric SmC^* phase, but in series 2 we observed both ferro- and antiferro-electric SmC^* phases, with the antiferroelectric SmC^* phase being predominant for early members of the series. The high melting points ($118\text{--}128^{\circ}\text{C}$) and small supercooling ranges ($6\text{--}10^{\circ}\text{C}$) found for series 1 compounds could mask any tendency for them to form antiferroelectric phases. For this reason we prepared a number of binary mixtures involving the octyloxy homologue from both series (compounds **7c** and **8c**) to investigate the tendency of series 1 compounds to form the antiferroelectric phase. A plot of transition temperature against various

compositions of binary mixtures of **7c/8c** are given in figure 6. It is clear that compound **7c** does not

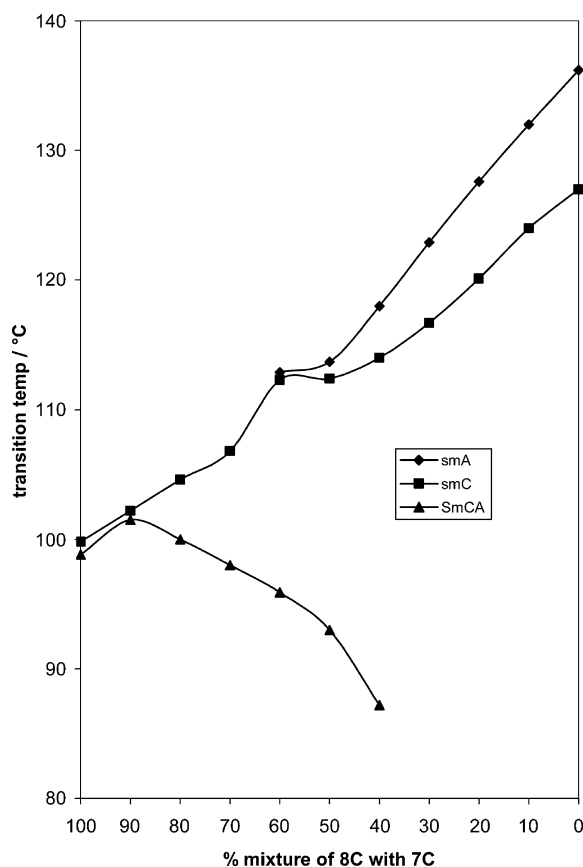


Figure 6. Plot of transition temperature against composition for binary mixtures of compounds **7c** and **8c**.

exhibit an antiferroelectric phase. We can conclude that series 1 compounds, as a whole, do not exhibit the antiferroelectric phase.

The incorporation of the pyrimidine ring has thus led to the formation of the antiferroelectric SmC* phase. The reasons for this could be both electronic and steric in nature. In series 1 the position of the two electron-donating moieties (the alkoxy group RO and the thiophene ring) with respect to the position of the electron-withdrawing ester group [–CO₂CH(CH₃)C₆H₁₃], renders the structure of these compounds bipolar. The bipolar structure of series 1 compounds is shown in figure 7(a). The appearance of the antiferroelectric phase in series 2 compounds could be due to the disruption of this bipolar structure by the incorporation of the electron-deficient pyrimidine ring. The thiophene ring is now flanked by two electron-withdrawing groups (the pyrimidine ring and the ester group), whereas the alkoxyphenyl ring is now adjacent to the electron-withdrawing pyrimidine ring, see figure 7(b). All these changes will increase the complexity of the electron distribution within the molecule, but the overall effect is that the series 2 structure will be less bipolar and more quadrupolar in nature than that for series 1.

Alternatively, the larger tilt angle found for series 2 compounds could influence the spatial arrangement of the terminal-positioned alkyl end chains at the layer interface, so that the mesogenic core favours an antiferroelectric rather than a ferroelectric arrangement. This idea was suggested by Yosizawa some years ago [12], but whether electronic or steric factors, or even a

combination of both, influence the formation of the antiferroelectric SmC* phase is very difficult to prove. However, what is certain is that the incorporation of a pyrimidine ring into a mesogenic structure can be conducive to the formation of the antiferroelectric SmC* phase.

One of the most striking effects has been on the melting points. Although the melting points for series 1 compounds are relatively low, around 120°C, for a three-ring mesogen the introduction of the pyrimidine ring in series 2 compounds lowered the melting points by a further 40–50°C. This produced compounds with exceptionally low melting points for three-ring mesogens. The overall effect of replacing the benzene ring by a pyrimidine ring is reminiscent of the effect caused by the incorporation of a lateral fluoro group. Lateral fluorination in a mesogen generally causes a sharp decrease in melting point and smectic thermal stability, but the effect is far less pronounced for the thermal stability of the SmC* phase [13–16]. In many cases the increased lateral polarity caused by the introduction of the laterally positioned fluoro group facilitates molecular tilting, and hence the formation of the SmC* phase. However, the effect of a lateral fluoro substituent is not always predictable and its position in the structure of the mesogen often determines its effect on the LC properties of the mesogen [17]. In series 2 compounds the nitrogen atoms of the pyrimidine ring, with their lone pair of electrons, are acting as the ‘laterally positioned fluoro substituent’, reducing both the melting point and SmA*/SmI* thermal stabilities but maintaining the SmC* phase. Like the fluoro substituent, the pyrimidine ring could play a key role in tailoring the important thermal and physical properties of LC materials.

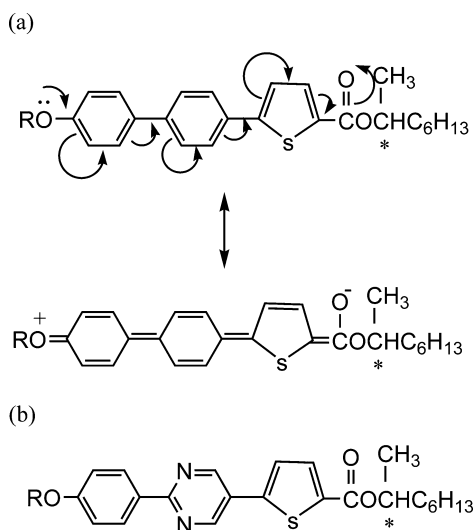


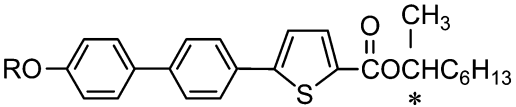
Figure 7. Possible electron distributions in (a) series 1 compounds and (b) series 2 compounds.

2.2. Electro-optical data on series 1 and 2 compounds

On cooling, crystallization for series 1 compounds appeared very quickly and so it was only possible to measure their tilt angles and P_s values at a reduced temperature of 5°C ($T_c - T/5^\circ\text{C}$), i.e. 5°C below the SmC*–SmA* transition. Many of the series 2 compounds crystallized some 20–30°C below the ferro- or antiferro-electric SmC*–isotropic transition, allowing their tilt angles and P_s values to be measured at various reduced temperatures: 5 ($T_c - T/5^\circ\text{C}$), 10 ($T_c - T/10^\circ\text{C}$) and 15 ($T_c - T/15^\circ\text{C}$)°C.

2.2.1. Series 1 compounds. As discussed earlier, it was during the electro-optical study that we found that these compounds exhibited the SmC*_z phase. On cooling from the SmA* phase we observed two peaks, which is typical of the SmC*_z phase. On approaching the

Table 3. Tilt angle and spontaneous polarization for series 1 compounds.



Compound <i>R</i>	Tilt angle/°	Spontaneous polarisation/nC cm ⁻² (T _c -T/5°C)
7a C ₆ H ₁₃	18	72
7b C ₇ H ₁₅	25.5	95
7c C ₈ H ₁₇	27.5	110
7d C ₉ H ₁₉	31	111
7e C ₁₀ H ₂₁	31.5	108
7f C ₁₁ H ₂₃	32	108
7g C ₁₂ H ₂₅	31.5	106

ferroelectric phase these two peaks converge and then become a single peak on passing into the ferroelectric phase. This sequence of events for compound **7e** is shown in figure 3. For compounds **7d–g**, the SmC_z* phase range is less than 2°C, but for compounds **7a–c**, the range is very small, around 0.1–0.2°C.

Because it was impossible to observe the SmC_z* phase by optical microscopy, all series 1 compounds were subjected to the electro-optical study. The tilt angles and P_s values at a reduced temperature of 5°C (T_c-T/5°C) for these compounds are given in table 3. Both the tilt angle and P_s values rise sharply with increase in size of the alkoxy group RO, but around the octyloxy/nonyloxy homologues, both the tilt angle and the P_s values remain fairly constant as the size of group RO increases. Typical tilt angle and P_s values for series 1 compounds are 31°–32° and 106–110 nC cm⁻², respectively.

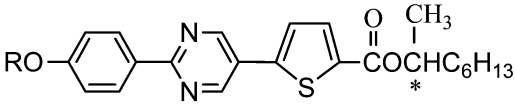
2.2.2. Series 2 compounds. Because all series 2 compounds supercool well below the clearing temperature, the electro-optical study for these compounds could be carried out at three reduced temperatures, 5, 10 and 15°C. The results from this study are given in table 4.

If we compare the data for both series of compounds at a reduced temperature of 5°C (T_c-T/5°C), clear differences between the two series of compounds can be seen. As for series 1, the tilt angle for series 2 compounds rises sharply as the size of the alkoxy group RO increases but at the octyloxy/nonyloxy homologues, it becomes fairly constant, giving series 2 compounds a typical tilt angle of 40°–41°. This is some 10° higher than that found for series 1 compounds. It is possible that the lone pair of electrons on the nitrogen atoms of the pyrimidine ring leads to enhanced interactions around the central part of the mesogenic core, forcing the molecules to tilt further to satisfy molecular packing in the layer plane.

Unlike series 1 compounds, the P_s values for series 2 decrease with increasing size of the alkoxy group RO; but again they tend to level off at the nonyloxy/decyloxy homologues, giving a typical P_s value for series 2 compounds of 180–190 nC cm⁻². These values are significantly higher, some 70–80 nC cm⁻², than those found for series 1 compounds.

The inverse relationship between tilt angle and P_s value (tilt angle increases but P_s decreases) with the size of the RO group for series 2 is unusual and difficult to understand. For a unit cell, increase in the tilt angle should manifest an increase in the P_s value due to the increase in population of molecules within the unit cell. One simple explanation could be that the presence of the pyrimidine ring enhances the bent nature of the 2, 5-disubstituent thiophene ring and so increases the overall molecular volume of the molecule. An increase in

Table 4. Tilt angle and spontaneous polarization for series 2 compounds.



Compound <i>R</i>	Tilt Angle/°C			Spontaneous Polarisation/nC cm ⁻²		
	T _c -T/5°C	T _c -T/10°C	T _c -T/15°C	T _c -T/5°C	T _c -T/10°C	T _c -T/15°C
8a C ₆ H ₁₃	36	37.5	38	210	225	235
8c C ₈ H ₁₇	39	40	40.5	180	203	225
8d C ₉ H ₁₉	40	40.5	40.5	179	192	205
8e C ₁₀ H ₂₁	40.5	41	41	160	178	190
8f C ₁₁ H ₂₃	41	41	41.5	170	185	192

molecular volume would certainly lead to a decrease in P_s value.

From the data presented in table 4 it can be seen that the tilt angle is fairly independent of temperature, especially for the higher homologues (nonyloxy onwards). A typical tilt angle for series 2 compounds is 40.5° – 41.5° , which is almost 10° higher than the tilt angles found for series 1 compounds. One possible reason for this could be the quadrupole-like distribution of molecular charge due to the presence of the pyrimidine ring, see figure 6(b). Such a charge distribution results in a high central core electron density, and so in the ferro- and antiferro-electric phases the molecules in the layered planes will tilt more to avoid repulsive interactions.

3. Conclusions

This study has shown the dramatic effect on both the thermal and physical properties of heterocyclic mesogens of replacing a phenyl ring by a pyrimidine ring. The inclusion of the pyrimidine ring is reminiscent of lateral fluorination; a reduction is seen in both the melting point and transition temperatures of the mesophases but with the melting point being most affected. Consequently, the thiophene-pyrimidine (series 2) compounds have relatively very low melting points for a three-ring mesogen, 70 – 85°C .

Both series of compounds exhibited the ferroelectric phase but only the series 2 compounds exhibited the antiferroelectric phase. It is clear from this work that the incorporation of a pyrimidine ring into the structure of a mesogen can be conducive to the formation of the antiferroelectric SmC^* phase.

The electro-optical helped to identify the SmC_z^* phase exhibited by members of series 1, and also showed that the incorporation of a pyrimidine ring gave mesogens with higher P_s values (200 – 230 nC cm^{-2}) and tilt angles (41° – 41.5°). One possible reason for this could be the disruption of the molecular electronic distribution, from a dipolar to a more quadrupolar-like distribution, by the incorporation of the pyrimidine ring.

The inverse relationship between tilt angle and P_s value (tilt angle increases but P_s value decreases) with the size of the *RO* group for series 2 compounds is unusual and difficult to understand.

4. Experimental

4.1. Characterization

^1H (400 MHz) and ^{13}C (100 MHz) nuclear magnetic resonance (NMR) spectra were obtained using the multinuclear JMN GX400FT spectrometer. All NMR

spectra were obtained in deuterated chloroform as solvent and with tetramethylsilane as internal standard. The following notations denote the peak types in the spectra: singlet (s), doublet (d), doublet of doublets (dd), triplet (t), quartet (q) and multiplet (m). Infrared spectra (IR) were obtained using a Perkin Elmer 983G spectrophotometer. Samples were prepared as potassium bromide discs. Mass spectra (MS) were obtained using a Finnigan 1020 GCMS spectrometer. In quoted results M^+ represents the molecular ion and the base peak is represented by (100%). Elemental analysis was carried out on a Fisons EA 1108 CHN instrument.

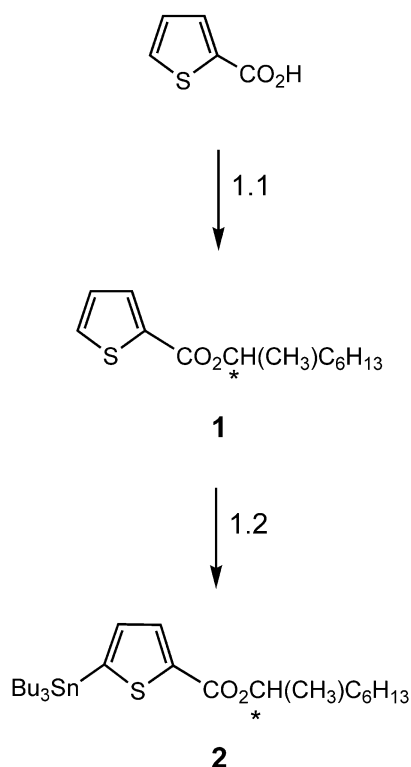
Differential scanning calorimetry (DSC) thermograms were obtained using a Perkin-Elmer DSC 7, with a TAC 7/PC interface and a controlled cooling accessory. The instrument was calibrated using an indium standard (m.p. 156.6°C , ΔH 28.45 J.g^{-1}). Heating and cooling rates were $10^\circ\text{C min}^{-1}$. Calculations were made using a Perkin-Elmer Pyris version 3.81 software. All the transitions are recorded as the onset temperature; for the crystal–mesophase transition this was taken on the heating cycle and for all other transitions on the cooling cycle.

Optical microscopy was performed using an Olympus BH-2 polarizing microscope, fitted with a Mettler FP52 hot stage and a Mettler FP5 controller. Samples were prepared as thin films between a glass slide and a glass cover slip, unless stated otherwise. Optical rotational measurements were obtained using an ETL-NPL automatic polarimeter control unit Type 143A. The sample was prepared in spectroscopy grade chloroform, and results are quoted at 25°C with a monochromatic sodium light source.

Column chromatography was carried out using Sorbsil C60 (40 – $60 \mu\text{m}$) as the stationary phase. Thin layer chromatography (TLC) was carried out on aluminium sheets coated in Merck Kieselgel silica gel 60 F_{254} , eluting with dichloromethane. HPLC was carried out on compounds **7a–g** and **8a–g** using a reverse phase Microsorb (Rainin Dynamax) column ($5 \mu\text{m}$, $25 \times 4.6 \text{ mm}^2$), eluting with a 9/1 mixture of acetonitrile/chloroform at 336 nm . The purity of all the compounds was $>99\%$.

4.2. Synthesis

The synthetic routes used for series 1 (**7a–g**) and 2 (**8a–g**) compounds are given in schemes 1 and 2, respectively. The synthesis of the intermediate 5-bromo-2-iodopyrimidine (scheme 2) has been discussed at some length in a previous paper [18]. Details of the preparation of compounds **3a–g**, **4a–g** and **6a–g** can be found in reference [1].



1.1 S-(+)-2-Octanol, DCC, DMAP, DCM

1.2 (i) LDA, THF; (ii) SnBu₃Cl, THF, - 78 °C

Scheme 1.

4.2.1. S-(+)-(1-Methylheptyl) thiophenecarboxylate 1.

To a stirred solution of 2-thiophenecarboxylic acid (22.5 g, 0.176 mol), S-(+)-2-octanol (22.9 g, 0.176 mol) and 4-dimethylaminopyridine (DMAP) (0.5 g) in dichloromethane (DCM) (350 ml) was added, dropwise, a solution of *N,N'*-dicyclohexylcarbodiimide (DCC) (36.3 g, 0.176 mol) in DCM (30 ml). The reaction mixture was stirred at room temperature, under an atmosphere of dry nitrogen, for 24 h. The contents of the flask were passed through a pad of silica gel and the solvent removed by distillation under reduced pressure to give a yellow oil. The crude product was purified by distillation under reduced pressure to afford compound **1** as a colourless oil, 33.7 g (80%), b.p. 134–7°C/3.0 mm Hg. δ_{H} (400 MHz, CDCl₃) 0.87 (t, 3H, *J* 7.2), 1.31 (m, 11H), 1.64 (m, 2H), 5.11 (sextet, 1H, *J* 7.2), 7.06 (dd, 1H, *J* 4.3, 2.7), 7.51 (dd, 1H, *J* 4.3, 2.7), 7.77 (dd, 1H, *J* 4.3, 2.7). δ_{C} (100 MHz, DEPT, CDCl₃) 13.5

(CH₃), 19.8 (CH₃), 22.4 (CH₂), 25.2 (CH₂), 28.9 (CH₂), 31.5 (CH₂), 35.8 (CH₂), 71.8 (CH), 127.4 (aromatic CH), 131.7 (aromatic CH), 132.7 (aromatic CH), 134.5 (quat. C), 161.6 (quat. C). MS *m/z* (EI) 240 (M⁺, 30%), 127 (41), 83 (100). $[\alpha]_{\text{D}}^{\text{20}}$ (CHCl₃, 20°C)=+38.1°. IR (KBr) ν_{max} 1712 cm⁻¹.

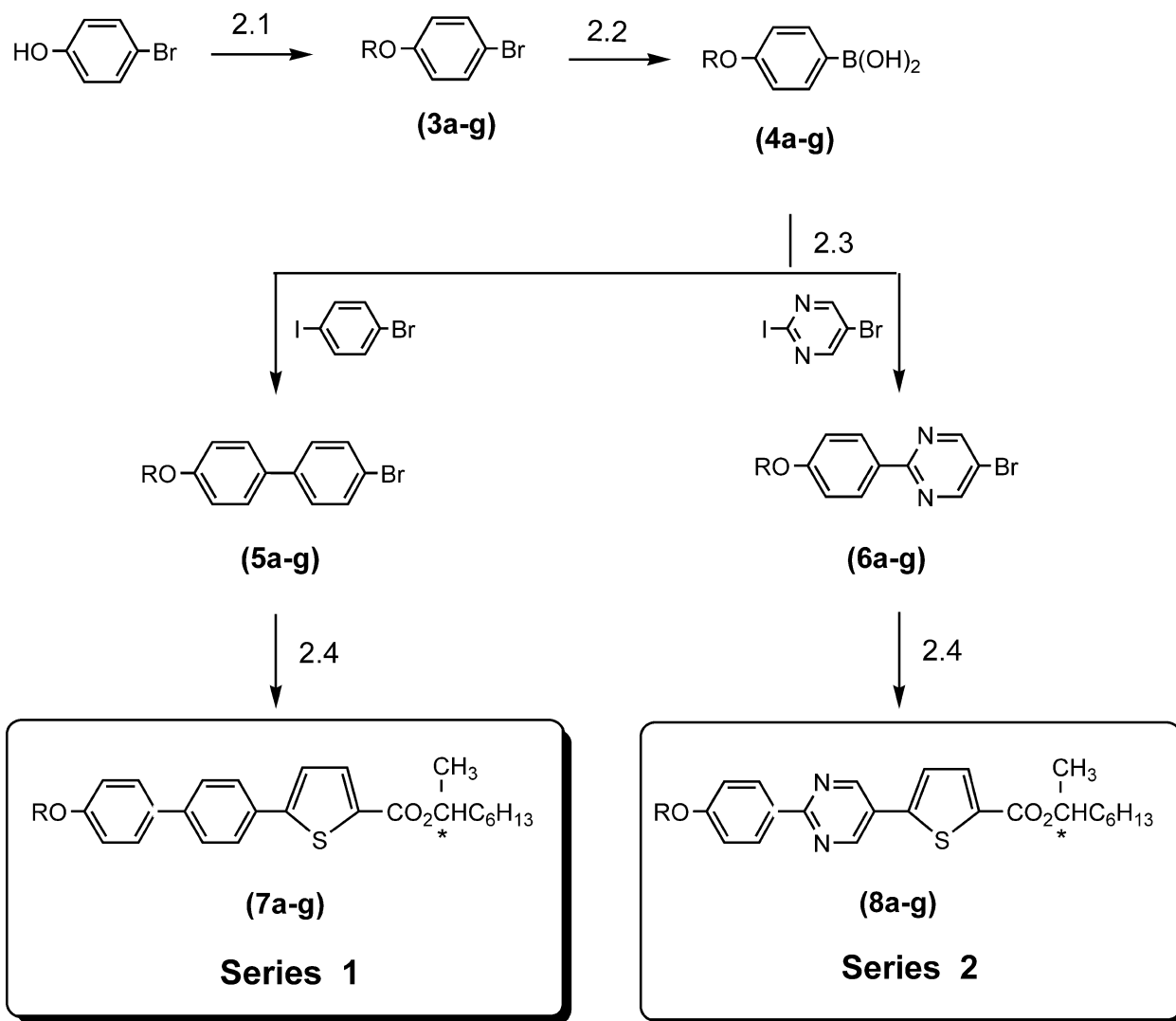
4.2.2. S-(+)-(1-Methylheptyl) 5-tri-*n*-butylstannylthiophene-2-carboxylate 2.

To a stirred solution of diisopropylamine (12.6 g, 0.125 mol) in dry THF (330 ml) at -78°C under an atmosphere of dry nitrogen was added, dropwise, *n*-butyllithium (50 ml, 2.5 M solution in hexanes, 0.125 mol). The reaction mixture was stirred for 1 h; a solution of compound **1** (30.0 g, 0.125 mol) in dry THF (30 ml) was then added dropwise, keeping the temperature below -70°C. After a further 1 h stirring a solution of tri-*n*-butylstannyl chloride (40.7 g, 0.140 mol) in dry THF (40 ml) was added dropwise, keeping the temperature below -70°C. After the addition, the reaction mixture was stirred at -78°C for 1 h, then allowed to reach room temperature overnight. It was then carefully quenched with water (250 ml) and the organic layer separated. The aqueous phase was washed with dichloromethane (3 × 250 ml) and the combined organic extracts were then dried (MgSO₄). Distillation under reduced pressure afforded compound **2** as a pale yellow oil, 46.5 g (70%), b.p. 236°C/1.5 mm Hg. δ_{H} (400 MHz, CDCl₃) 0.89 (t, 12H, *J* 7.2 Hz), 1.13 (m, 5 H), 1.32 (m, 18H), 1.57 (m, 8H), 5.10 (sextet, 1H, *J* 7.2), 7.14 (d, 1H, *J* 4.3), 7.86 (d, 1H, *J* 4.3). δ_{C} (100 MHz, DEPT, CDCl₃) 10.8 (3 × CH₂), 13.5 (4 × CH₃), 14.0 (CH₃), 20.0 (CH₂), 22.9 (CH₂), 25.3 (CH₂), 27.2 (3 × CH₂), 28.7 (3 × CH₂), 31.8 (CH₂), 35.9 (CH₂), 71.7 (CH), 133.6 (aromatic CH), 135.6 (aromatic C), 139.7 (quat. C), 146.7 (quat. C), 166.8 (quat. C). $[\alpha]_{\text{D}}^{\text{20}}$ (CHCl₃, 20°C)=+24.7°. IR (KBr) ν_{max} 1714 cm⁻¹.

4.2.3. 4-Bromo-4'-hexyloxybiphenyl 5a.

A stirred mixture of 1-bromohexane (7.2 g, 43.9 mmol), 4-bromo-4'-hydroxybiphenyl (10.0 g, 40.3 mmol), anhydrous potassium carbonate (15.5 g, 112.3 mmol) and potassium iodide (0.5 g) in butanone (150 ml) was heated under reflux for 24 h. The potassium salts were removed by hot filtration and the solvent removed by distillation under reduced pressure. The crude product was recrystallized (butanone) to give compound **5a** as a white solid, 12.1 g (90%), m.p. 128°C (Lit [19] 128.5°C). δ_{H} (400 MHz, CDCl₃) 0.88 (t, 3H), 1.33 (m, 4H), 1.46 (m, 2H), 1.79 (quin, 2H), 3.97 (t, 2H), 6.95 (d, 2H), 7.39 (d, 2H), 7.45 (d, 2H), 7.51 (d, 2H). MS *m/z* 376–374 (M⁺), 250, 248, 233, 231, 182, 168, 152.

The remaining 4-bromo-4'-alkyloxybiphenyls **5b–g** were prepared using the same general procedure as



2.1 K₂CO₃, butanone, appropriate alkyl bromide

2.2 (i) Mg, THF; (ii) B(OCH₃)₃, THF, -78 °C; (iii) H⁺

2.3 Pd(PPh₃)₄, NaCO₃, H₂O, DME

2.4 compound **2**, PdCl₂(PPh₃)₂, DMF

3-8a, R = C₆H₁₃; 3-8b, R = C₇H₁₅; 3-8c, R = C₈H₁₇; 3-8d, R = C₉H₁₉; 3-8e, R = C₁₀H₂₁; 3-8f, R = C₁₁H₂₃; 3-8g, R = C₁₂H₂₅

Scheme 2.

described for **5a**. All the materials were obtained as white solids and yields were in the range 80–84%. IR and ^1H NMR spectra were found to be consistent with the structure of each compound and similar to that obtained for **5a**, except that in the case of the ^1H NMR spectra, the integration of the appropriate multiplets reflected the additional methylene ($-\text{CH}_2-$) groups. **5b**: m.p. 127°C (Lit. [19] 126.5°C). MS m/z 348–346 (M^+), 250, 248, 233, 231, 182, 168, 152. **5c**: m.p. 125–126°C (Lit. [19] 125.5°C). MS m/z 362–360 (M^+), 250, 248, 233, 231, 182, 168, 152. **5d**: m.p. 122–123°C (Lit. [19] 123°C). MS m/z 376–374 (M^+), 250, 248, 233, 231, 182, 168, 152. **5e**: m.p. 122°C (Lit. [19] 121°C). MS m/z 390–388 (M^+), 250, 248, 233, 231, 182, 168, 152. **5f**: m.p. 117°C. MS m/z 404–402 (M^+), 250, 248, 233, 231, 182, 168, 152. **5g**: m.p. 114°C (Lit. [19] 115°C). MS m/z 418–416 (M^+), 250, 248, 233, 231, 182, 168, 152.

4.2.4. S-(+)-1-Methylheptyl 5-(4-hexyloxybiphenyl-4'-yl)thiophene-2-carboxylate, 7a. To a stirred solution of compound **5a** (1.35 g, 4.0 mmol) and compound **2** (2.10 g, 4.0 mmol) in dry DMF (50 ml) at 100°C under an atmosphere of dry nitrogen, bis(triphenylphosphine)palladium(II) chloride (0.1 g) was added, and the reaction mixture stirred for 24 h. The DMF was removed by distillation under reduced pressure and the crude material purified, firstly by flash column chromatography (silica gel, DCM) and then further by column chromatography (silica gel, 2/1 DCM/petroleum ether, b.p. 40–60°C) and then recrystallized (ethanol). To remove metal ions, the product was treated with charcoal, underwent column chromatography (alumina, DCM) and was finally passed through a syringe filter (0.02 μm) to yield compound **7a** as a pale yellow crystalline solid, 1.2 g (61%). δ_{H} (400 MHz, CDCl_3) 0.90(m, 6H), 1.35(m, 16H), 1.66(m, 2H), 1.75(m, 3H), 4.50(t, 2H), 5.11(sext, 1H), 6.97(d, 2H), 7.30(d, 1H), 7.55(d, 2H), 7.58(d, 2H), 7.68(d, 2H), 7.75(d, 1H). IR (KBr) ν_{max} 2928, 1698, 1449, 1290, 1099, 810 cm^{-1} . MS m/z 492 (M^+), 380, 296, 279, 250, 234, 152. Calc. for $\text{C}_{31}\text{H}_{40}\text{O}_3\text{S}$, C 75.60, H 8.13, S 6.50; found, C 75.60, H 8.27, S 6.60%. $[\alpha]_{\text{D}} (c. 0.00745 \text{ g ml}^{-1}) = +40.14^\circ$.

The remaining S-(+)-1-methylheptyl 5-(4-alkyloxybiphenyl-4'-yl)thiophene-2-carboxylates **7b–g** were prepared using the same general procedure as described for compound **7a**, i.e. using 2.10 g of compound **2**. All the materials were obtained as pale yellow crystalline solids and yields were in the range 57–80%. IR and ^1H NMR spectra were found to be consistent with the structure of each compound and similar to that obtained for **7a**. The only exception was in the case of the ^1H NMR spectra, where the integration of the appropriate multiplets reflected the additional methylene ($-\text{CH}_2-$)

groups. **7b**: MS m/z 506 (M^+), 394, 296, 279, 250, 234, 152. Calc. for $\text{C}_{32}\text{H}_{42}\text{O}_3\text{S}$, C 75.85, H 8.35, S 6.33; found, C 75.70, H 8.65, S 6.13%. $[\alpha]_{\text{D}} (c. 0.00820 \text{ g ml}^{-1}) = +39.39^\circ$. **7c**: MS m/z 520 (M^+), 408, 296, 279, 250, 234, 152. Calc. for $\text{C}_{33}\text{H}_{44}\text{O}_3\text{S}$, C 76.15, H 8.46, S 6.15; found, C 76.44, H 8.76, S 6.24%. $[\alpha]_{\text{D}} (c. 0.0421 \text{ g ml}^{-1}) = +34.1^\circ$. **7d**: MS m/z 534 (M^+), 422, 296, 279, 250, 234, 152. Calc. for $\text{C}_{34}\text{H}_{46}\text{O}_3\text{S}$, C 76.36, H 8.67, S 6.00; found, C 76.27, H 8.97, S 5.83%. $[\alpha]_{\text{D}} (c. 0.018620 \text{ g ml}^{-1}) = +38.54^\circ$. **7e**: MS m/z 548 (M^+), 436, 296, 279, 250, 234, 152. Calc. for $\text{C}_{35}\text{H}_{48}\text{O}_3\text{S}$, C 76.60, H 8.75, S 5.84; found, C 76.80, H 8.97, S 5.92%. $[\alpha]_{\text{D}} (c. 0.01037 \text{ g ml}^{-1}) = +39.22^\circ$. **7f**: MS m/z 562 (M^+), 450, 296, 279, 250, 234, 152. Calc. for $\text{C}_{36}\text{H}_{50}\text{O}_3\text{S}$, C 76.82, H 8.95, S 5.70; found, C 76.75, H 9.25, S 5.44%. $[\alpha]_{\text{D}} (c. 0.00638 \text{ g ml}^{-1}) = +33.75^\circ$. **7g**: MS m/z 576 (M^+), 464, 296, 279, 250, 234, 152. Calc. for $\text{C}_{37}\text{H}_{52}\text{O}_3\text{S}$, C 77.08, H 9.03, S 5.56; found, C 77.06, H 9.29, S 5.30%. $[\alpha]_{\text{D}} (c. 0.000605 \text{ g ml}^{-1}) = +35.59^\circ$.

4.2.5. S-(+)-1-Methylheptyl 5-[2-(4-hexyloxyphenyl)pyrimid-5-yl]thiophene-2-carboxylate, 8a. To a stirred solution of 5-bromo-2-(4-hexyloxyphenyl)pyrimidine **6a** (1.4 g, 4.1 mmol) and compound **2** (2.10 g, 4.0 mmol) in dry DMF (50 ml) at 100°C under an atmosphere of dry nitrogen, bis(triphenylphosphine)palladium(II) chloride (0.2 g) was added, and the reaction mixture stirred for 24 h. The DMF was removed by distillation under reduced pressure and the crude material purified, firstly by flash column chromatography (silica gel, DCM) and then further by column chromatography (silica gel, 2/1 DCM/petroleum ether, b.p. 40–60°C) and then recrystallized (ethanol). To remove metal ions, the product was treated with charcoal, underwent column chromatography (alumina, DCM) and was finally passed through a syringe filter (0.02 μm) to give compound **8a** as a pale yellow crystalline solid, 1.3 g (65%). δ_{H} (400 MHz, CDCl_3) 0.90(m, 6H), 1.35(m, 16H), 1.60(m, 2H), 1.75(m, 3H), 4.05(t, 2H), 5.13(sext, 1H), 7.0(d, 2H), 7.38(d, 1H), 7.81(d, 1H), 8.41(d, 2H), 8.98(s, 2H). IR (KBr) ν_{max} 2928, 1695, 1426, 1286 cm^{-1} . MS m/z 494 (M^+), 410, 298, 280, 252, 209, 152. Calc. for $\text{C}_{29}\text{H}_{38}\text{N}_2\text{O}_3\text{S}$, C 70.41, H 7.74, N 5.66, S 6.48; found, C 70.66, H 7.92, N 5.65, S 6.31%. $[\alpha]_{\text{D}} (c. 0.10208 \text{ g ml}^{-1}) = +45.38^\circ$.

The remaining S-(+)-1-methylheptyl 5-[2-(4-alkyloxyphenyl)pyrimid-5-yl]thiophene-2-carboxylates **8b–g** were prepared using the same general procedure as described for **8a**, i.e. using 2.10 g of compound **2**. All the materials were obtained as pale yellow crystalline solids and the yields were in the range 50–68%. The IR and ^1H NMR spectra were found to be consistent with the structure of each compound and similar to that

obtained for **8a**, except that in the case of the ^1H NMR spectra, the integration of the appropriate multiplets reflected the additional methylene ($-\text{CH}_2-$) groups. **8b**: MS m/z 508(M^+), 410, 298, 280, 252, 209, 152. Calc. for $\text{C}_{30}\text{H}_{40}\text{N}_2\text{O}_3\text{S}$, C 70.83, H 7.93, N 5.51, S 6.30; found, C 70.95, H 8.13, N 5.50, S 6.10%. $[\alpha]_{\text{D}}$ (c. 0.02172 g ml^{-1}) = $+42.96^\circ$. **8c**: MS m/z 522(M^+), 410, 298, 280, 252, 209, 152. Calc. for $\text{C}_{31}\text{H}_{42}\text{N}_2\text{O}_3\text{S}$, C 71.23, H 8.10, N 5.36, S 6.13; found, C 71.51, H 8.31, N 5.36, S 5.87%. $[\alpha]_{\text{D}}$ (c. 0.01979 g ml^{-1}) = $+41.10^\circ$. **8d**: MS m/z 536(M^+), 410, 298, 280, 252, 209, 152. Calc. for $\text{C}_{32}\text{H}_{44}\text{N}_2\text{O}_3\text{S}$, C 71.60, H 8.26, N 5.22, S 5.97; found, C 71.90, H 8.42, N 5.24, S 5.72%. $[\alpha]_{\text{D}}$ (c. 0.01992 g ml^{-1}) = $+39.63^\circ$. **8e**: MS m/z 550(M^+), 410, 298, 280, 252, 209, 152. Calc. for $\text{C}_{33}\text{H}_{46}\text{N}_2\text{O}_3\text{S}$, C 71.96, H 8.42, N 5.09, S 5.82; found, C 72.24, H 8.72, N 5.04, S 6.19%. $[\alpha]_{\text{D}}$ (c. 0.01892 g ml^{-1}) = $+38.13^\circ$. **8f**: MS m/z 564(M^+), 410, 298, 280, 252, 209, 152. Calc. for $\text{C}_{34}\text{H}_{48}\text{N}_2\text{O}_3\text{S}$, C 72.30, H 8.57, N 4.96, S 5.68; found, C 72.39, H 8.83, N 5.01, S 5.60%. $[\alpha]_{\text{D}}$ (c. 0.01292 g ml^{-1}) = $+37.03^\circ$. **8g**: MS m/z 578(M^+), 410, 298, 280, 252, 209, 152. Calc. for $\text{C}_{35}\text{H}_{50}\text{N}_2\text{O}_3\text{S}$, C 72.62, H 8.71, N 4.84, S 5.54; found, C 72.89, H 9.00, N 4.72, S 5.35%. $[\alpha]_{\text{D}}$ (c. 0.00698 g ml^{-1}) = $+37.70^\circ$.

4.3. The electro-optic study

The cells used in this study were $5\text{ }\mu\text{m}$ antiparallel rubbed polyimide cells purchased from Linkam, with an active area of 0.81 cm^2 . They were prepared using the following procedure. The cell was flow filled with sample by capillary action and wires attached using indium. The temperature was controlled by a Mettler FP82HT heating stage in conjunction with a Mettler FP90 temperature controller. The compounds were aligned in the cells from the isotropic state with a cooling rate of $0.2^\circ\text{C min}^{-1}$ under the application of a square waveform at 1 KHz and $20\text{ V }\mu\text{m}^{-1}$, although with some materials alignment was achieved with a more rapid cooling rate. A Hewlett Packard (HP33120A) wave generator was used, and the waveform amplified by a linear X20 amplifier (designed and constructed by QinetiQ). The resultant signals were observed using a Hewlett Packard (HP54600B) oscilloscope connected to a PC through an RS232 port.

4.3.1. Measurement of P_s values. P_s values were determined using the current reversal technique. Once the material was aligned in the cell, the temperature was taken to just above the Curie point; or if there was no phase above the SmC*, the temperature was taken close to the isotropization point and the waveform changed

from a square waveform to a triangular waveform at 30 Hz and $10\text{ V }\mu\text{m}^{-1}$. The resultant signal from the switch was represented on the oscilloscope as a current pulse, and once the signal wave was averaged-out to remove the noise, the sample was downloaded into a computer programme (HP Benchlink) through the RS232 port. The current response was then transferred to another programme (P_s and Optical Response, M. Watson, Hull University, 1994) where the area under the current pulse peak could be calculated and the P_s value determined. The P_s measurements were carried out at 1°C intervals until the sample underwent a phase transition to a higher ordered, more viscous phase or crystallized.

4.3.2. Measurement of tilt angles. The tilt angle was determined by taking the aligned sample to just above the Curie point or close to the clearing point for the case where there was no phase above the SmC* phase and applying a square waveform at 30 Hz and $10\text{ V }\mu\text{m}^{-1}$. The sample was rotated and the minimum in transmittance for the switched states was determined using a photodiode (RS303-674; 1 cm^2 active area, high speed $<50\text{ ns}$) in an apparatus designed by QinetiQ. The angle through which the sample had been rotated gave the cone angle and hence the tilt angle. The tilt angle was determined at 1°C intervals.

Acknowledgements

We would like to thank the EPSRC and COMIT for funding R.M. and the EPSRC for funding S.C. We would also like to thank Professor J.W. Goodby for help in the identification of the SmI* phase by optical microscopy.

References

- [1] S. Sharman, D. Lacey, S. Cowling. *Liq. Cryst.*, **30**, 451 (2003).
- [2] D. Demus, J. Deresch, L. Richter, A. Wiegeleben. *Mol. Cryst. Liq. Cryst.*, **59**, 329 (1980).
- [3] S.M. Kelly, J. Funfschilling. *Liq. Cryst.*, **19**, 195 (1995).
- [4] J. Funfschilling, M. Schadt. *Jpn. J. appl. Phys.*, **30**, 741 (1991).
- [5] M. Schadt. *Liq. Cryst.*, **14**, 73 (1993).
- [6] Y. Aoki, H. Nohira. *Liq. Cryst.*, **19**, 15 (1995).
- [7] A.J. Seed, M. Hird, P. Styring, H. Glesson, J.T. Mills. *Mol. Cryst. liq. Cryst.*, **299**, 19 (1997). A.J. Seed, K.J. Toyne, J.W. Goodby and M. Hird. *J. mater. Chem.*, **10**, 2069 (2000).
- [8] A. Matharu, R.C. Wilson, C. Grover. *Mol. Cryst. liq. Cryst.*, **332**, 303 (1999). A.S. Matharu, C. Grover, L. Komitov and G. Andersson. *J. mater. Chem.*, **10**, 1303 (2000).
- [9] D.J. Byron, L. Komitov, A.S. Matharu, I. McSherry, R.C. Wilson. *J. mater. Chem.*, **6**, 1871 (1996).
- [10] I. Nishiyama. *Ad. Mater.*, **6**, 966 (1994).

- [11] L.S. Hirst, S.J. Watson, H.F. Gleeson, P. Cluzeau, P. Barois, R. Pindak, J. Pitney, A. Cady, P.M. Johnson, C.C. Huang, A.-M. Levelut, G. Srajer, J. Pollmann, W. Caliebe, A. Seed, M.R. Herbert, J.W. Goodby, M. Hird. *Phys. Rev. E*, **65**, 041705 (2002).
- [12] (a) A. Yoshizawa, I. Nishiyama, H. Kikuzaki and N. Ise. *Jpn J. appl Phys*, **31**, L860 (1992); (b) A. Yoshizawa, N.A. Yokoyama, H. Kikuzaki and T. Hirai. *Liq. Cryst.*, **14**, 513 (1993); (c) A. Yoshizawa, H. Kikuzaki and M. Fukumasa. *Liq. Cryst.*, **18**, 351 (1995).
- [13] L.K.M. Chan, G.W. Gray, D. Lacey, K.J. Toyne. *Mol. Cryst. liq. Cryst.*, **158B**, 209 (1988).
- [14] G.W. Gray, M. Hird, D. Lacey, K.J. Toyne. *J. chem. Soc., Perkin Trans. 2*, 2337 (1989).
- [15] T. Kusumoto, K. Ogino, K. Sato, T. Hiyama, S. Takehara, K. Nakamura. *Chem. Lett.*, 1243 (1993).
- [16] M. Hird, K.J. Toyne. *Mol. Cryst. liq. Cryst.*, **323**, 1 (1998).
- [17] V. Reiffenrath, J. Krause, H.J. Plach, G. Weber. *Liq. Cryst.*, **5**, 159 (1989).
- [18] R.A. Lewis, M. Hird, J.W. Goodby, K.J. Toyne. *Chem. Commun.*, 2719 (1996).
- [19] G.W. Gray, K.J. Harrison, J.A. Nash, J. Constant, P.S. Hulme, J. Kirton, E.P. Raynes. *Liq. Cryst. ordered Fluids*, **2**, 617 (1974).